Available online at www.sciencedirect.com
ScienceDirect
Polymer 48 (2007) 5928–5939
polymer
www.elsevier.com/locate/polymer

Foaming of polymers with supercritical CO_2: An experimental and theoretical study

Ioannis Tsivintzelis, Anastasia G. Angelopoulou, Costas Panayiotou*

Laboratory of Physical Chemistry, Department of Chemical Engineering, Aristotle University of Thessaloniki, 54124 Thessaloniki, Greece

Received 2 April 2007; received in revised form 31 July 2007; accepted 2 August 2007
Available online 8 August 2007

Abstract

Microcellular polystyrene (PS) foams and porous structures of the biodegradable poly(D,L-lactic acid) ($P_{D,L}LA$) were prepared with the batch foaming technique (pressure quench) using supercritical CO_2 as blowing agent. The effect of pressure, temperature and depressurization rate on the final porous structure was investigated. The results revealed that the size of the pores decreases and their population density increases with pressure increase, or decrease of temperature, and/or increase of the depressurization rate. The results were correlated by combining nucleation theory with NRHB model in order to account for and emphasize the physical mechanism related to nucleation of bubbles inside the supersaturated polymer matrix. A satisfactory agreement between correlations and experimental data was obtained indicating that the nucleation theory yields quantitative correlations when variables such as sorption, degree of plasticization, and surface tension of the system polymer–supercritical fluid are accurately described.

Keywords: Foams; Nucleation; Supercritical CO_2

1. Introduction

Recently, various supercritical fluid processing methods have been developed for the production of polymer-based materials such as foams, microparticles, membranes and fibers [1]. In this direction, cellular polymers can be formed through the gas foaming technique. According to this method, the polymer is saturated with a gas or supercritical fluid (usually CO_2 or N_2) at constant temperature and pressure. Then, the system is brought to the supersaturated state either by reducing pressure (pressure induced phase separation) or by increasing temperature (temperature induced phase separation) resulting in the nucleation and growth of pores – cells inside the polymer matrix [2,3]. In amorphous polymers, usually the growth of the pores continues until the polymer vitrifies [3,4].

Foaming of polymers with gases or supercritical fluids allowed the successful production of microcellular polymers. Such structures consist of pores with diameter smaller than 10 μm and population density larger than 10^9 cells per cm^3 [5]. Compared to compact materials, these foams exhibit significant advantages. They offer reduced bulk density that induces materials' saving and decreases transportation cost. On the other hand, they often exhibit high impact strength, high toughness, high stiffness-to-weight ratio, high fatigue life as well as low dielectric constant and low thermal conductivity [5]. These unique properties indicate microcellular polymers as candidate materials for many industrial applications, which include airplane and automotive parts, sporting equipment, acoustic dampening, thermal insulation, microelectronic applications and optical devices [6].

Furthermore, foaming of polymers with gases or supercritical fluids exhibits a strong advantage especially in the processing of polymers for various biomedical applications. There is no need for use of harmful organic solvents that in most cases are not easily removed from the final product

* Corresponding author. Tel.: +30 2310 996223; fax: +30 2310 996232.
E-mail address: cpanayio@auth.gr (C. Panayiotou).

0032-3861/$ - see front matter © 2007 Elsevier Ltd. All rights reserved.
doi:10.1016/j.polymer.2007.08.004

material [7]. Porous structures of biocompatible and biodegradable polymers are used as scaffolds in tissue engineering, which, among others, is aiming at the regeneration of damaged tissue [8]. Scaffolds, which provide a temporary artificial matrix for cell seeding, should meet certain fundamental characteristics such as high porosity, appropriate pore size, biocompatibility, biodegradability and proper degradation rate [8]. Consequently, scaffold fabrication methods should allow for the control of pore size and enhance the maintenance of mechanical properties and materials' biocompatibility.

The foaming of many polymers with gaseous or supercritical CO_2 has been investigated. Poly(methyl methacrylate) [3,9], polystyrene [4,10], polycarbonate [11] and poly(ethylene terephthalate) [12] are among the most studied polymers. In some cases, the method was applied for the foaming of biodegradable polymers such as poly(lactic-*co*-glycolic acid) [7,13], poly(ε-caprolactone) [14–16] and polylactic acid [17,18].

The modelling of bubble nucleation inside the polymer matrix is usually performed on the basis of classical nucleation theory [19,20]. Nevertheless, with this approach the nucleation activity is often not accurately described when the foaming occurs with temperature induced phase separation [5]. On the other hand, homogeneous nucleation theory proved able to describe reasonably the effect of pressure and temperature on nucleation when the foaming is performed with pressure induced phase separation [3,6]. According to Goel and Beckman, the latter happens because, prior to the pressure quench, the system (polymer and dissolved gas) is in a homogeneous liquid state (usually much higher pressure is exercised than needed for the plasticization of the polymer matrix at the operating temperature) [3]. Nevertheless, often the process is only qualitatively described and not accurate correlations are yielded rendering the modelling of bubble nucleation inside the polymer matrix as a challenging task.

Modelling of bubble nucleation requires an accurate description of many complex processes, such as the sorption of CO_2 and the induced plasticization of the polymer matrix or the interfacial tension between the metastable polymeric phase and the newly developed gas nuclei. In the absence of extended experimental data there is a need for accurate prediction of these properties by an appropriate model.

In this direction, Siripurapu et al., who studied the foaming of PMMA films, used the Sanchez–Lacombe equation of state and a proper extension of the theory to interfaces in order to predict sorption and interfacial tension [6]. They combined the model with the nucleation theory and correlated the experimental cell population densities with improved accuracy.

Recently, the Non-Random Hydrogen-Bonding (NRHB) theory of fluids has been proposed [21,22]. It is an equation of state model that can be applied to liquid, vapor, as well as to supercritical state. Also, it is applicable to complex systems and processes such as polymer solutions, sorption of gases or supercritical fluids into polymers, as well as to fluid interfaces. In combination with Gibbs–DiMarzio proposition, it can be used to elucidate complex phenomena such as the plasticization of glassy polymers, including the retrograde vitrification.

Porous polystyrene structures are used in many industrial applications which include packaging, acoustic and thermal insulation materials. On the other hand, polylactic acid lies among the most common polymers for bioengineering applications and its porous structures are often used as scaffolds in tissue engineering [8,23]. In the present study, microcellular polystyrene (PS) foams and porous structures of the biodegradable poly(D,L-lactic acid) ($P_{D,L}LA$) were prepared with the batch foaming technique (pressure induced phase separation). The effect of pressure, temperature and depressurization rate on the final porous structure was investigated. The results were discussed in the framework of classical nucleation theory, which was applied in combination with NRHB model.

2. Experimental

2.1. Materials

PS ($M_w = 230\,000$, $M_w/M_n = 2.1$) was purchased from BDH, $P_{D,L}LA$ ($M_w = 189\,000$, $M_w/M_n = 2.8$, 12% D(−) content) was purchased from Gelactic and CO_2 from Air Liquide Mediterranée (>99.98% purity). All materials were used as received and without any further purification.

2.2. Preparation of porous structures

Pellets of the raw material were dried overnight at 55 °C under vacuum. Discs with 15 mm diameter and uniform thickness of 0.75 mm were prepared by compression-molding the polymer at 150 and 80 °C for PS and $P_{D,L}LA$, respectively. The experimental apparatus, which is described elsewhere [15], consists of a high pressure syringe pump (ISCO, model 100DX) and a thermostated pressure vessel (ISCO, model SFX™ 2-10). In each experiment, one compression-molded disc was placed inside the pressure vessel and the latter was immediately filled with CO_2 at the desired temperature and pressure. The system remained at these conditions at least for 4 h and then it was rapidly depressurized by opening a needle valve. In this study, the mean pressure drop rate of each experiment is reported.

2.3. Characterization

Polymers were characterized by differential scanning calorimetry (Shimadzu DSC-50). PS exhibits glass-to-rubber transition around 103.8 °C and $P_{D,L}LA$ around 52.1 °C.

All produced porous samples were fractured in liquid nitrogen and their cross-sections were studied by scanning electron microscopy (JEOL, model JSM-840A). All surfaces were coated with carbon to avoid charging under the electron beam. The pore size distributions were obtained by image analysis with the use of appropriate software.

The bulk density of the foamed samples was measured by the buoyancy method (ASTM D-792) with triethylene glycol as liquid with known density. Liquid uptake in the foamed samples was not observed due to the dense skin surrounding the porous structure.

The cell density (number of cells per unit of volume) was correlated considering spherical pores from the following equation:

$$N_c = \frac{6}{\pi}\frac{1}{d^3}\left(1-\frac{\rho_f}{\rho_p}\right) \quad (1)$$

where d is the mean pore diameter, ρ_f the foam density and ρ_p the neat polymer density.

3. Theory

3.1. Nucleation theory

According to the nucleation theory, in a closed isothermal system in chemical equilibrium the difference of the free energy per unit volume related to the formation of new phase cluster is given by the following equation [24,25]:

$$\Delta G = -\frac{4\pi r^3}{3}\Delta P + 4\pi r^2\gamma \quad (2)$$

where r is the radius of the spherical cluster, γ is the interfacial tension, and ΔP is the pressure difference between the two sides of the interface. Eq. (2) is derived assuming homogeneous nucleation and also that the new phase cluster has properties as a bulk phase in the same physical state. It reflects the sum of the gain in the free energy related to the formation of the new phase and the cost of the free energy due to the introduction of the interface.

When ΔG is plotted against cluster size, one obtains a curve that shows a maximum at a critical radius r_c:

$$\frac{d\Delta G}{dr} = 0 \Rightarrow r_c = \frac{2\gamma}{\Delta P} \quad (3)$$

Eq. (3) is the well known Young–Laplace equation. The maximum value of ΔG for homogeneous nucleation is obtained by substituting Eq. (3) into Eq. (2), or:

$$\Delta G^*_{hom} = \frac{16\pi\gamma^3}{3\Delta P^2} \quad (4)$$

The rate of nucleation can be described by the following equation [3]:

$$N_o = C_0 f_0 \exp\left(\frac{-\Delta G^*_{hom}}{kT}\right) \quad (5)$$

where C_0 is the concentration of the dissolved fluid inside the polymer matrix (expressed as number of molecules per volume), k the Boltzman constant and T the temperature. The parameter f_0 is a frequency factor for the gas molecules, which describes the rate at which nuclei with critical radius are transformed into stable bubbles [24]. This frequency factor can be expressed as a function of the critical radius [3]:

$$f_o = ZR_{imp}\left(4\pi r_c^2\right) \quad (6)$$

In this equation, Z is the Zeldovich factor and R_{imp} the rate of impingement of the gas molecules per unit area.

As proposed by Goel and Beckman [3], the total number of nuclei that are generated during the nucleation time is calculated by the integration of the nucleation rate, N_o:

$$N_{total} = \int_0^{t,vitr} N_o\, dt = \int_{P,sat}^{P,vitr} N_o \frac{dP}{dP/dt} \quad (7)$$

where the sat and vitr denote saturation and vitrification, respectively.

According to Eqs. (4)–(7), in order to apply the nucleation theory, the amount of the dissolved fluid, the induced plasticization of the polymer matrix, and the interfacial tension are required. Consequently, in the absence of extended experimental data there is a need of an appropriate model.

3.2. NRHB model

In what follows, we will summarize the essential formalism of the NRHB model. Details may be found elsewhere [21,26]. According to this model, the molecules are assumed to be arranged on a quasi-lattice of coordination number z and of N_r sites, N_0 of which are empty. Each fluid of type i in the system is characterized by three Lattice-Fluid scaling constants and one geometric or surface-to-volume-ratio factor. The three scaling constants are: the mean interaction energy per segment, ε^*_i, the hard-core volume per segment, v^*_i, and the hard-core density, $\rho^*_i = 1/v^*_{sp,i}$. Each molecule occupies r_i sites of the quasi-lattice and has $q_i = s_i r_i$ external intermolecular constants, where s_i is its geometric factor. The number of sites r_i is given by:

$$r_i = \frac{Mw_i\, v^*_{sp,i}}{v^*_i} \quad (8)$$

where Mw_i is the molecular weight of the i component.

Similar scaling constants, indicated without subscript, are defined for the mixture through the following combining and mixing rules:

$$\varepsilon^* = P^* v^* = RT^* = \theta_1^2\varepsilon_1^* + \theta_2^2\varepsilon_2^* + 2\theta_1\theta_2\varepsilon_{12}^*, \quad (9)$$

$$\varepsilon_{12}^* = (1-k_{12})\sqrt{\varepsilon_1^*\varepsilon_2^*} \quad (10)$$

$$v^* = \phi_1^2 v_1^* + 2\phi_1\phi_2 v_{12}^* + \phi_2^2 v_2^* \quad (11)$$

$$v_{12}^* = \left(\frac{v_1^{*1/3} + v_2^{*1/3}}{2}\right)^3 \quad (12)$$

where k_{12} is a binary interaction parameter, while the site fractions ϕ_i and the surface fractions θ_i are defined as following:

$$\phi_i = \frac{r_i N_i}{rN} = \frac{x_i r_i}{r} \quad (13)$$

and

$$\theta_i = \frac{q_i N_i}{\sum_k q_k N_k} = \frac{q_i N_i}{qN} = \frac{\phi_i s_i}{\sum_k \phi_k s_k} = \frac{\phi_i s_i}{s} \tag{14}$$

where

$$r = \sum_i x_i r_i \tag{15}$$

while x_i is the mole fraction of component i.

In order to correlate phase equilibrium, one needs the equation of state and the equations for the chemical potentials of each component i at different phases. The equation of state has the following form [21,26]:

$$\tilde{P} + \tilde{T}\left[\ln(1-\tilde{\rho}) - \tilde{\rho}\left(\sum_i \phi_i \frac{l_i}{r_i}\right) - \frac{z}{2}\ln\left(1 - \tilde{\rho} + \frac{q}{r}\tilde{\rho}\right) + \frac{z}{2}\ln \Gamma_{00}\right] = 0 \tag{16}$$

while the chemical potential for component i is given by [21,26]:

$$\begin{aligned}\frac{\mu_i}{RT} = {} & \ln\frac{\phi_i}{\omega_i r_i} - r_i \sum_j \frac{\phi_j l_j}{r_j} + \ln\tilde{\rho} + r_i(\tilde{v}-1)\ln(1-\tilde{\rho}) \\ & - \frac{z}{2} r_i\left[\tilde{v} - 1 + \frac{q_i}{r_i}\right]\ln\left[1 - \tilde{\rho} + \frac{q}{r}\tilde{\rho}\right] \\ & + \frac{z q_i}{2}\left[\ln \Gamma_{\mathrm{rr}} + \frac{r_i}{q_i}(\tilde{v}-1)\ln \Gamma_{00}\right] - \frac{q_i}{\tilde{T}} \\ & - r_i \frac{\tilde{P}\tilde{v}}{\tilde{T}}\left[1 - \frac{2}{v^*}\sum_j \phi_j v^*_{ij}\right] \\ & + \frac{2 q_i \Theta_r \Gamma_{\mathrm{rr}}}{RT}\left[\varepsilon^* - \sum_j \theta_j \varepsilon^*_{ij}\right]\end{aligned} \tag{17}$$

where

$$\tilde{T} = \frac{T}{T^*},\ \tilde{P} = \frac{P}{P^*},\ \tilde{\rho} = \frac{\rho}{\rho^*} = \frac{1}{\tilde{v}} \tag{18}$$

$$l_i = \frac{z}{2}(r_i - q_i) - (r_i - 1) \tag{19}$$

and

$$\Theta_r = 1 - \Theta_0 = \frac{q/r}{q/r + \tilde{v} - 1} \tag{20}$$

ω_i is a characteristic quantity for each fluid i that takes into account the flexibility and symmetry of the molecule. Furthermore, Γ_{00} and Γ_{rr} are factors for the non-random distribution of empty sites around an empty site and for the distribution of molecular segments around a central molecular segment, respectively. These non-randomness factors are obtained through Guggenheim's quasi-chemical condition and are given by:

$$\begin{aligned}\Theta_0 \Gamma_{00} + \Theta_r \Gamma_{r0} &= 1 \\ \Theta_r \Gamma_{\mathrm{rr}} + \Theta_0 \Gamma_{r0} &= 1\end{aligned} \tag{21}$$

and

$$\Gamma_{r0} = \frac{2}{1 + [1 - 4\Theta_0\Theta_r(1-A)]^{1/2}} \tag{22}$$

where

$$A = \frac{\Gamma_{\mathrm{rr}}\Gamma_{00}}{\Gamma_{r0}^2} = \exp\left(\frac{2\varepsilon^*/z}{RT}\right) \tag{23}$$

The determination of the sorption-induced plasticization, namely the pressure (or the concentration) of the gas at a specific temperature, for which glass transition occurs, can be achieved by adopting Gibbs–DiMarzio rationale [27]. According to this the total entropy of the system becomes zero at the glass transition. The entropy of a binary system is obtained from the equation:

$$\begin{aligned}\frac{S}{rNR} = {} & \sum_i \frac{\phi_i}{r_i}\ln\delta_i + (1-\tilde{v})\ln(1-\tilde{\rho}) + \frac{l + \ln(r\tilde{v}) - \sum_i x_i \ln x_i}{r} \\ & + \frac{z}{2}\left[\tilde{v} - 1 + \frac{q}{r}\right]\ln\left[1 - \tilde{\rho} + \frac{q}{r}\tilde{\rho}\right] + \frac{zq}{2r}\left[\theta_0 \Gamma_{r0}\frac{2\varepsilon^*}{zRT} - \ln \Gamma_{\mathrm{rr}}\right] \\ & - \frac{z}{2}(\tilde{v}-1)\ln \Gamma_{00}\end{aligned} \tag{24}$$

where

$$l = \sum_i x_i l_i, \tag{25}$$

$$\ln\delta_i = \ln(Z/2) - (r_i - 2)\ln(1 - f_i) + f_i(r_i - 2)\frac{u_i}{RT}, \tag{26}$$

$$f_i = \frac{(Z-2)\exp\left(-\frac{u_i}{RT}\right)}{1 + (Z-2)\exp\left(-\frac{u_i}{RT}\right)} \tag{27}$$

In these equations δ is the number of different configurations available to the chain of the polymeric fluid, Z is the number of discrete conformations available to each bond and f is the fraction of the $r-2$ bonds of the chain molecule that is in high-energy states. Finally, u is the increase of the intramolecular energy that accompanies the "flexing" of a bond in the chain molecule. This "flex" energy is a characteristic parameter of each polymer and is calculated usually by zeroing S at the glass transition temperature of the neat polymer at ambient pressure.

The interfacial tension between two phases a and b at equilibrium is obtained from the following equation [21]:

$$\gamma = (2 + \beta)\int_{\rho^a}^{\rho^b} [c\Delta\psi_0]^{1/2} \mathrm{d}\rho \tag{28}$$

where

$$c = \varepsilon^* (v^*)^{5/3} \kappa \tag{29}$$

In these equations γ is the interfacial tension, ρ the density and ψ_o the Helmholtz free energy density. Parameters β and κ are characteristic for each fluid [21].

4. Results and discussion

Uniform cross-sections were observed for all the produced PS and $P_{D,L}LA$ porous structures. The porous core was surrounded by a dense unfoamed skin (at the edges of the sample). This is a typical behaviour in the foaming of polymers with gases or supercritical fluids. According to Goel and Beckman the formation of a dense nonporous skin results due to the rapid diffusion of the dissolved fluid from the sample edges [28]. The molecules of the blowing agent, that are sorbed near the edges, diffuse out of the sample faster than they can join nuclei. Representative porous structures are presented in Figs. 1 and 2 for the PS and $P_{D,L}LA$, respectively.

4.1. Effect of pressure

The effect of pressure on the final porous structure was studied at constant temperature and using a constant depressurization rate. PS porous structures were produced at two temperatures, 80 and 100 °C, while pressure ranged between 180 and 380 bar. $P_{D,L}LA$ porous structures were produced at 35 °C, while pressure varied between 70 and 200 bar. In all cases the depressurization was taking place quickly, in less than 20 s.

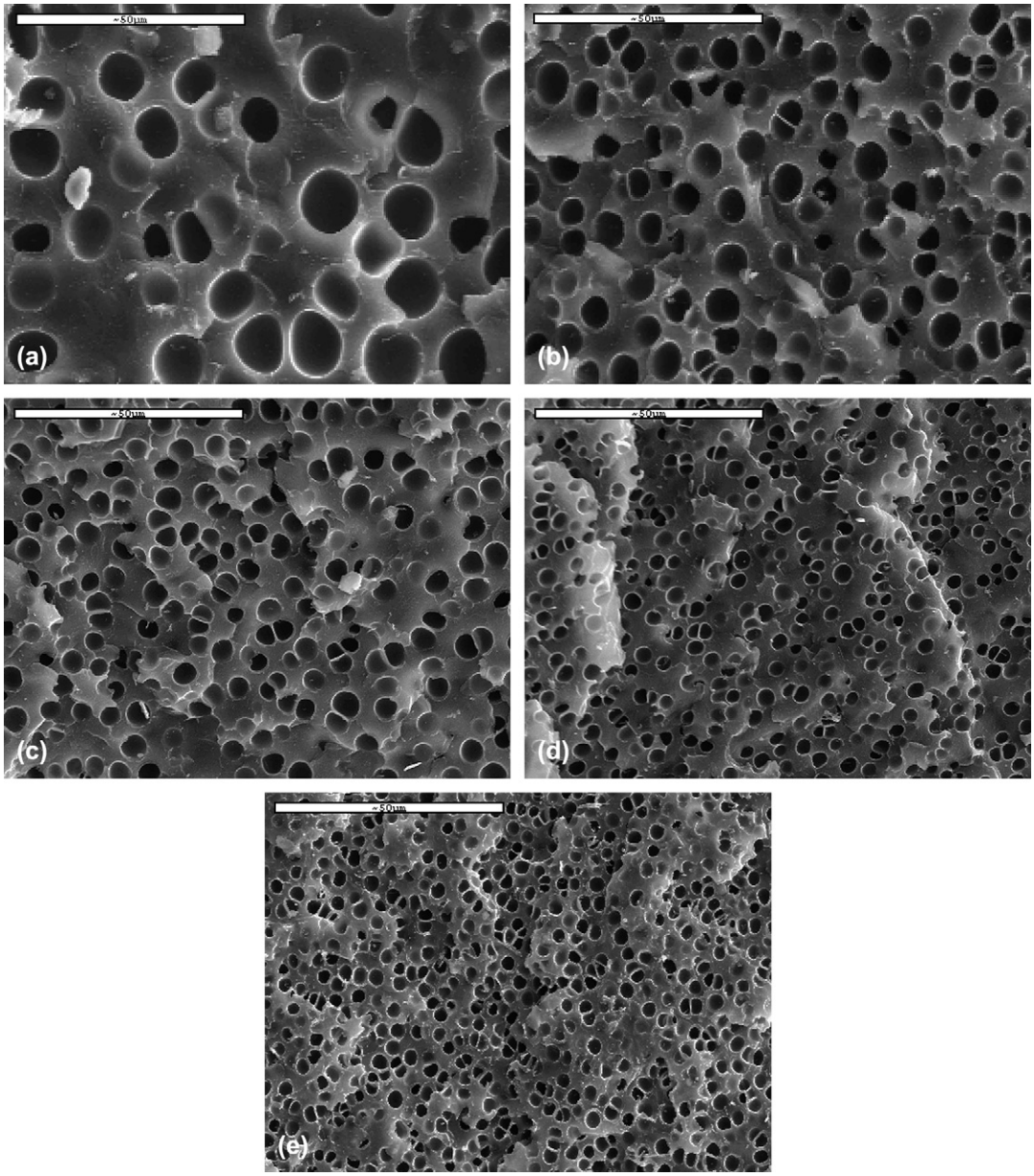

Fig. 1. Porous PS structures (temperature: 80 °C; pressure: (a) 180, (b) 230, (c) 280, (d) 330, (e) 380 bar; depressurization time: <20 s).

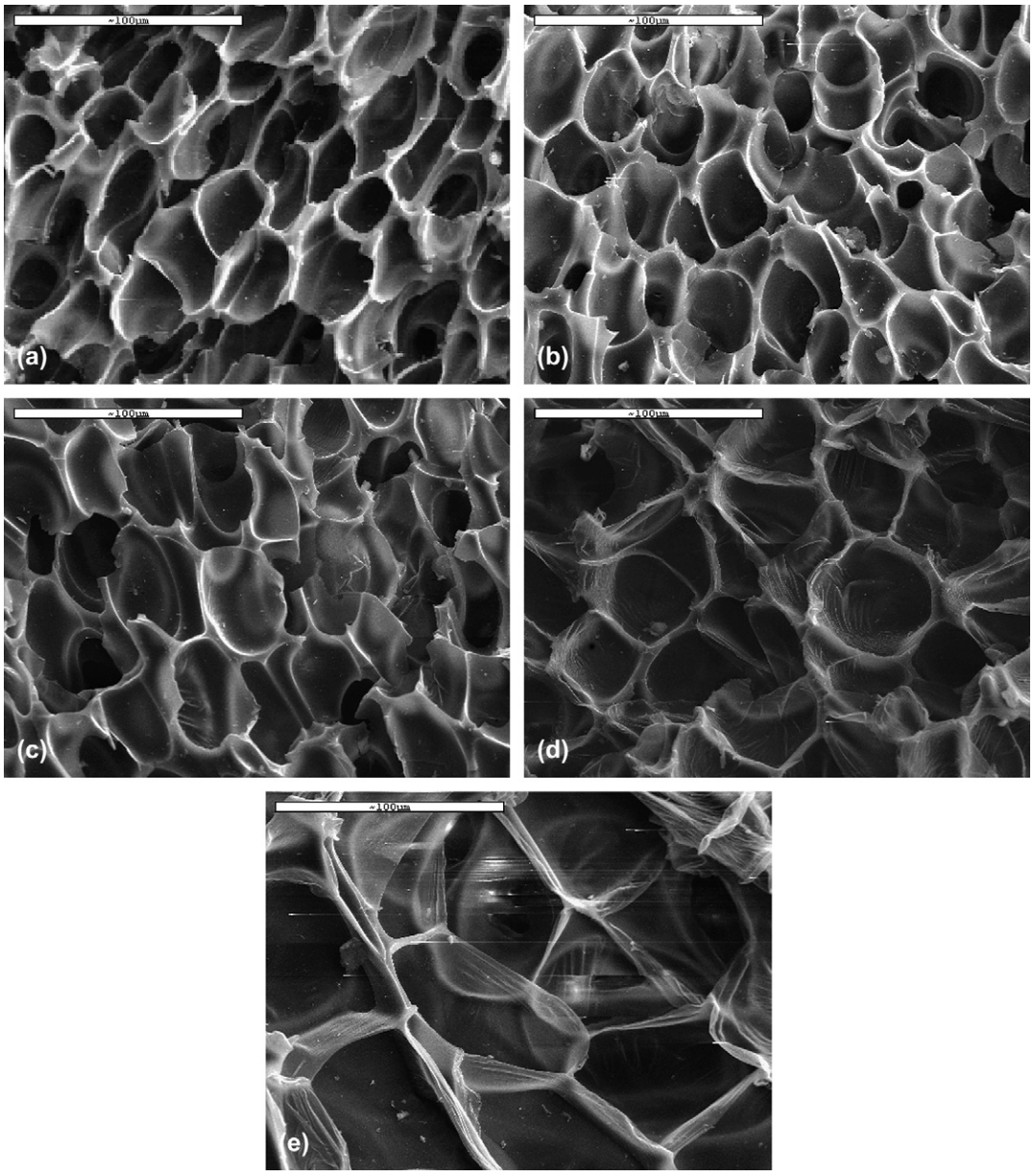

Fig. 2. Porous $P_{D,L}LA$ structures (temperature: (a) 35, (b) 40, (c) 45, (d) 50, (e) 55 °C; pressure: 150 bar; depressurization time: <20 s).

As presented in Figs. 3–6 the mean pore diameter and the bulk foam density decreased, while the cell density increased with increase of pressure. At constant temperature, as the pressure increases, more fluid is dissolved into the polymer matrix and causes more pronounced plasticization and viscosity reduction. More pronounced plasticization implies that the interval between saturation and vitrification pressure is increased, while the viscosity reduction facilitates the growth of pores. The longer period that cells have to grow before vitrification, coupled with easier growth due to viscosity reduction, trend towards the formation of larger pores [3,4]. Nevertheless, the experimental results indicate that these effects are likely negligible. The key factor that controls the cell size is the generation of more nuclei as pressure increases, which in turn leads to structures with increased cell density (see Figs. 5 and 6). In other words, when larger pressure is applied not only there is more dissolved fluid into the polymer matrix available for the nucleation and growth of pores, but also a larger number of nuclei (that should share this fluid) are formed. Consequently, much more cells with smaller size are produced [3,4]. Finally, the decrease in the bulk foam density that is observed in Figs. 5 and 6 could be attributed to the enhancement of the fluid solubility into the polymer matrix.

As shown in Figs. 3 and 5, microcellular PS structures were produced in most cases.

4.2. Effect of temperature

The effect of temperature on the final porous structure was studied at constant pressure and using constant depressurization

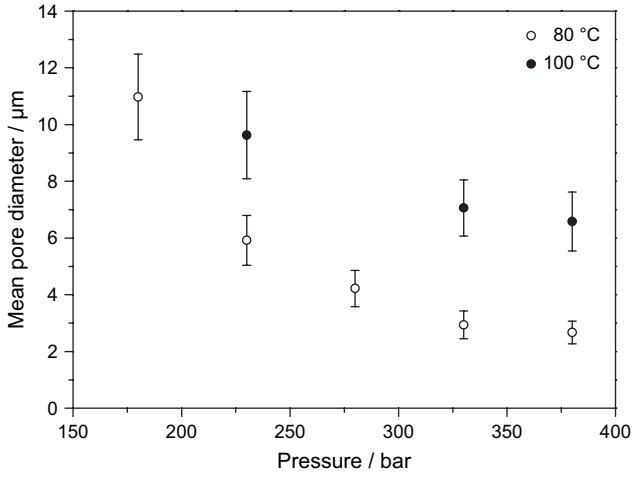

Fig. 3. Effect of pressure on the final pore size for PS.

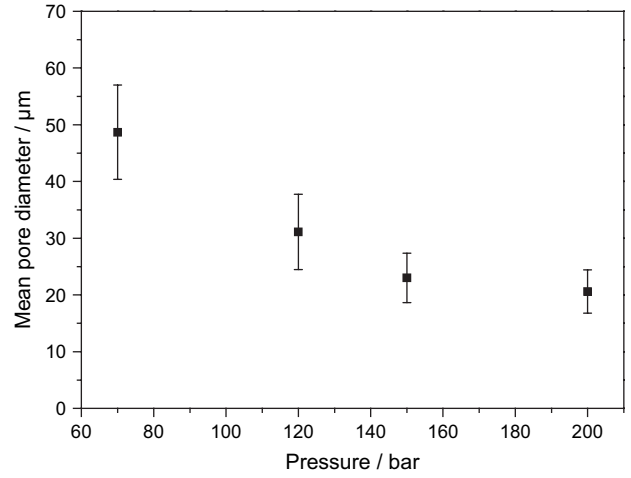

Fig. 4. Effect of pressure on the final pore size for $P_{D,L}LA$ at 35 °C.

rate. PS porous structures were produced at 330 bar, while temperature ranged between 80 and 120 °C. $P_{D,L}LA$ porous structures were produced at 150 bar, while temperature varied between 35 and 55 °C. In all cases the depressurization was taking place quickly, in less than 20 s.

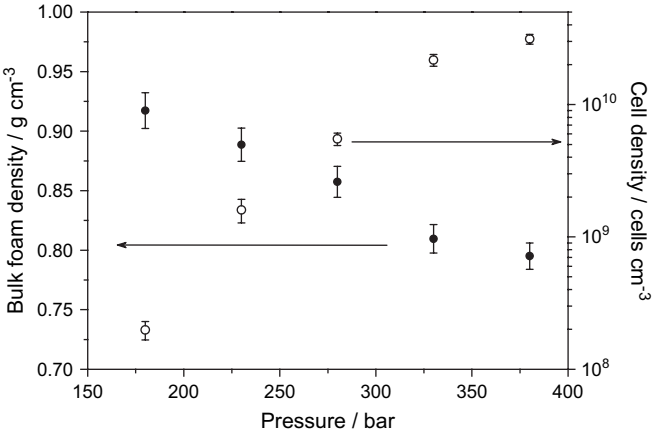

Fig. 5. Effect of pressure on the bulk foam and cell density for PS at 80 °C.

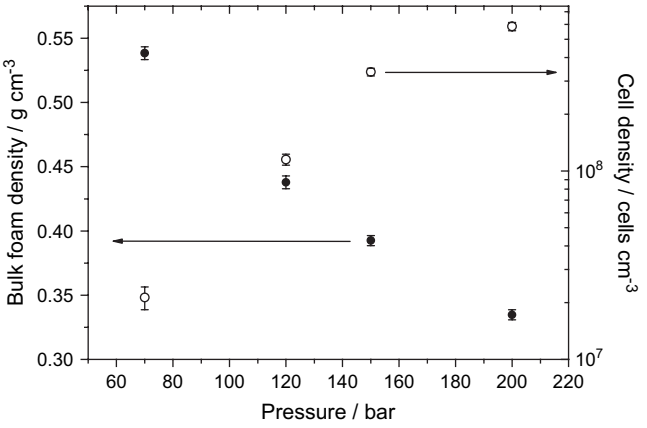

Fig. 6. Effect of pressure on the bulk foam and cell density for $P_{D,L}LA$ at 35 °C.

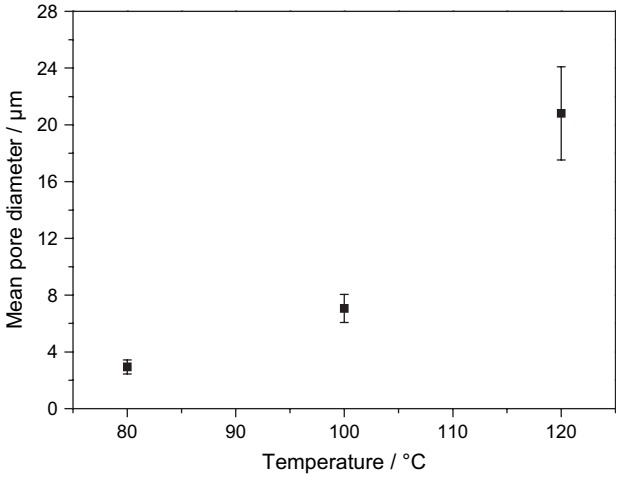

Fig. 7. Effect of temperature on the final pore size for PS at 330 bar.

As presented in Figs. 7–10 the mean pore diameter increased, while the bulk foam density and the cell population

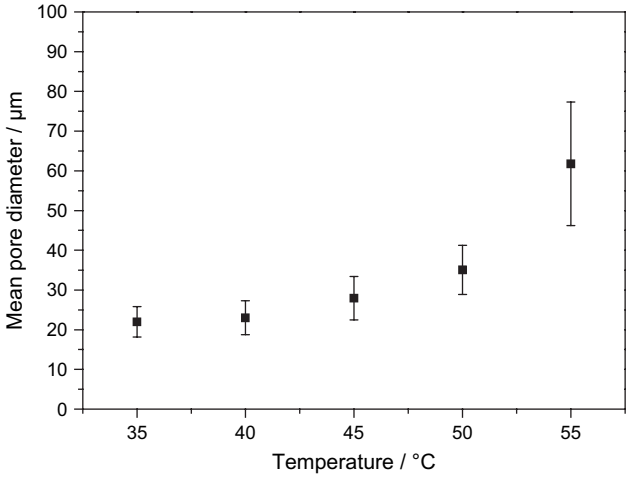

Fig. 8. Effect of temperature on the final pore size for $P_{D,L}LA$ at 150 bar.

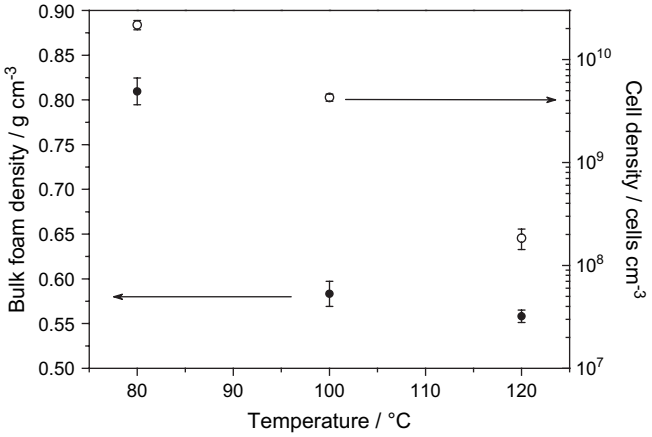

Fig. 9. Effect of temperature on the bulk foam and cell density for PS at 330 bar.

density decreased with increase of temperature. When foaming occurs at higher temperatures, the CO_2 diffusivity is increased rendering the cell growth faster. Also, the interval between saturation and vitrification pressure is increased resulting in longer growth periods which in turn lead to the formation of larger cells and foams with reduced bulk density [3]. Finally, as the temperature increases, the CO_2 solubility in the polymer matrix decreases. Also the cell density decreases as indicated in Figs. 9 and 10. In other words, at higher temperatures there is less dissolved fluid into the polymer matrix available for the nucleation and growth of pores, but fewer nuclei (that should share this fluid) are formed. The net effect of all these factors is an exponential increase in the pore size with increase in temperature.

4.3. Effect of depressurization rate

The effect of depressurization rate on the final porous structure was studied at constant temperature and pressure. PS porous structures were obtained at 80 °C and 330 bar, while $P_{D,L}LA$ porous structures were obtained at 35 °C and

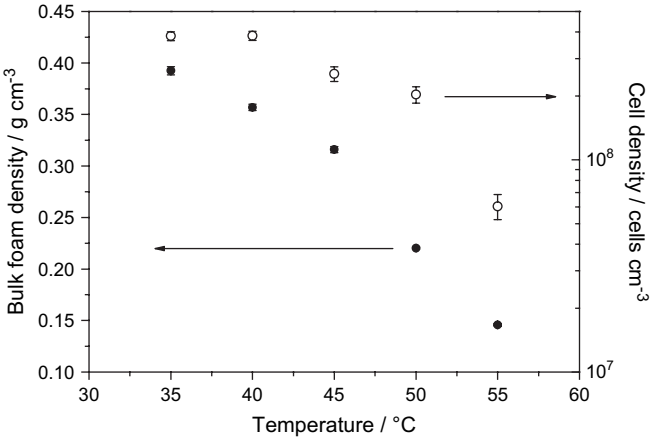

Fig. 10. Effect of temperature on the bulk foam and cell density for $P_{D,L}LA$ at 330 bar.

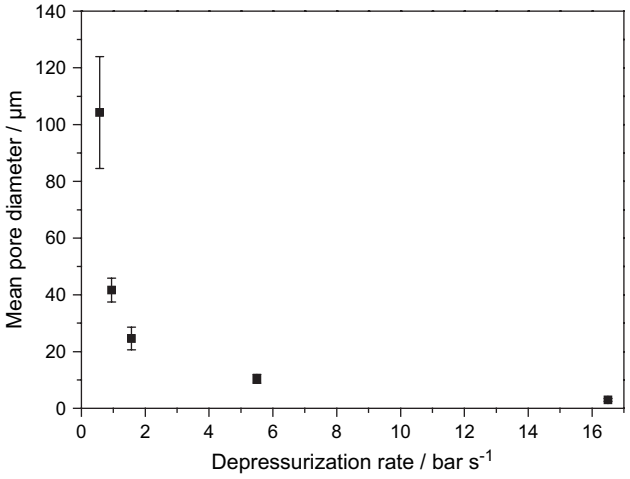

Fig. 11. Effect of depressurization rate on the final pore size for PS at 80 °C and 330 bar.

150 bar. Keeping a constant depressurization rate is a very difficult experimental task, mainly, due to the CO_2 density change [29]. In this study, the mean pressure drop rate of each experiment is reported.

As presented in Figs. 11–14, the mean pore diameter decreased, while the cell population density increased with increase of the depressurization rate. This could be attributed to the coalescence of neighboring cells that is thermodynamically favored due to the reduction of the interfacial area [4]. At lower depressurization rates the growth period of pores – the time period between nucleation and "locking" of the porous structure due to vitrification – is larger. Consequently, the coalescence of neighboring pores is more pronounced.

Furthermore, Guo et al. used a high pressure vessel equipped with a visualization window and applied an appropriate image analysis in order to study the effect of depressurization rate on nucleation [29]. The authors report that at higher pressure drop rates, more gas is used for cell nucleation instead for cell growth. Consequently, at higher depressurization rate more

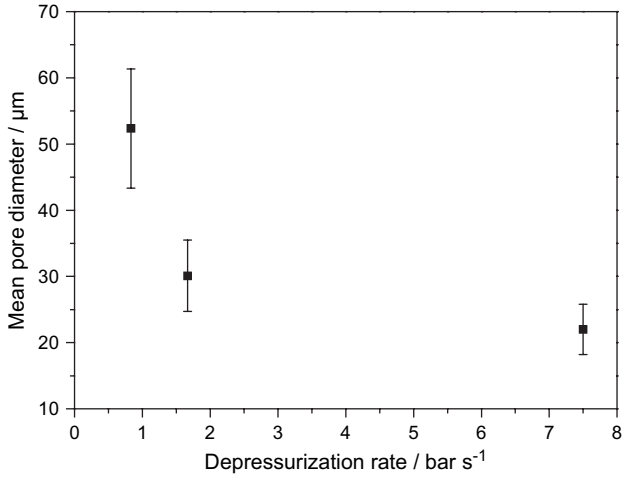

Fig. 12. Effect of depressurization rate on the final pore size for $P_{D,L}LA$ at 35 °C and 150 bar.

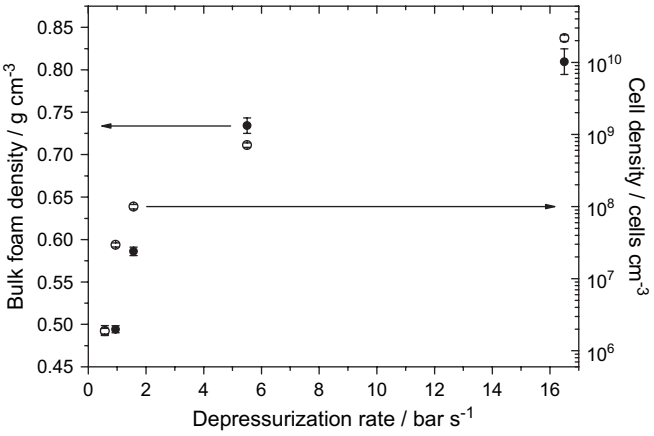

Fig. 13. Effect of depressurization rate on the bulk foam and cell population density for PS at 80 °C and 330 bar.

nuclei are generated resulting in the formation of more pores with smaller size.

4.4. Theoretical correlations

According to Eqs. (2)–(5), the nucleation rate depends on the amount of the dissolved fluid, the induced plasticization of the polymer matrix and the interfacial tension between the metastable polymeric phase and a gas bubble.

Contrary to the system $P_{D,L}LA-CO_2$, the system PS–CO_2 has been thoroughly investigated. The sorption of supercritical CO_2 in atactic PS and the induced plasticization of the polymer matrix have been reported in many studies [4,26,30,31]. On the other hand, experimental data for the interfacial tension of polymer–supercritical fluid systems are rather rare and refer to temperatures higher than those usually applied in the batch foaming procedure. Nevertheless, surface tension of polystyrene melts in supercritical CO_2 was measured at temperatures between 210 and 230 °C [32,33]. Due to the absence of experimental data, nucleation theory was not applied for the system $P_{D,L}LA-CO_2$. Nucleation theory was only used for the

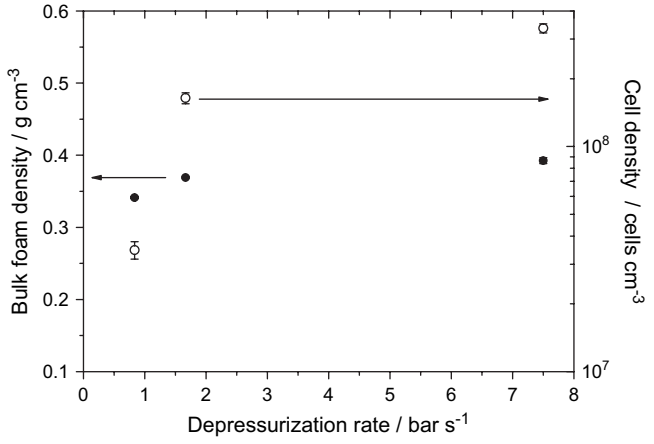

Fig. 14. Effect of depressurization rate on the bulk foam and cell population density for $P_{D,L}LA$ at 35 °C and 150 bar.

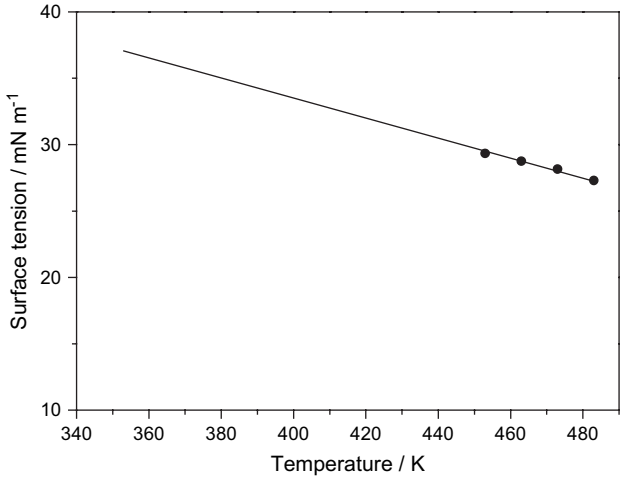

Fig. 15. Surface tension of polystyrene: (●) experimental data [33]; (—) NRHB.

correlation of the experimental results that refer to the foaming of PS.

In order to estimate the interfacial tension, the polymer matrix after the CO_2 dissolution was considered as a homogeneous liquid mixture. Considering that the surface tension of a supercritical fluid is essentially zero, the mixture's surface tension was calculated from the following empirical equation [34]:

$$\gamma_{\mathrm{mix}}^{1/r} = (1 - w_{\mathrm{CO_2}})\gamma_{\mathrm{pol}}^{1/r} \tag{30}$$

where γ is the surface tension and w_{CO_2} the weight fraction of the dissolved fluid. Subscripts mix and pol denote the mixture and the pure polymer, respectively. The parameter r was estimated to be equal to 13 by fitting the experimental data [33]. On the other hand, the surface tension of the pure polymer, the sorption of CO_2 at the foaming temperatures, and the plasticization of the polymer matrix were correlated using NRHB model. The results are illustrated in Figs. 15–17. The NRHB pure fluid scaling parameters are presented in Table 1

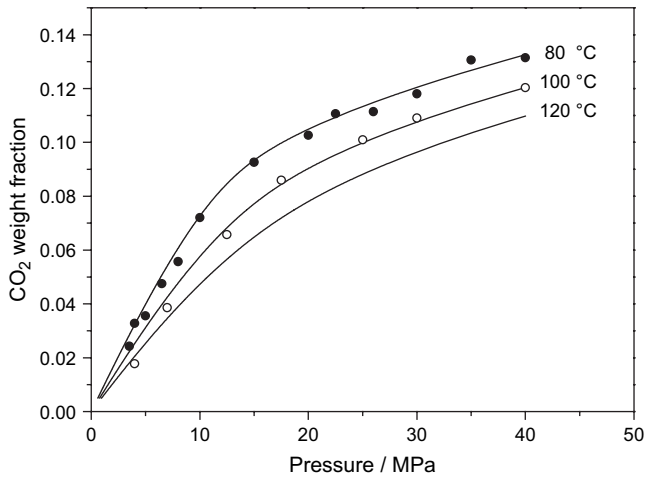

Fig. 16. CO_2 sorption in polystyrene, experimental data [26]: (○) 100 °C; (●) 80 °C; (—) NRHB.

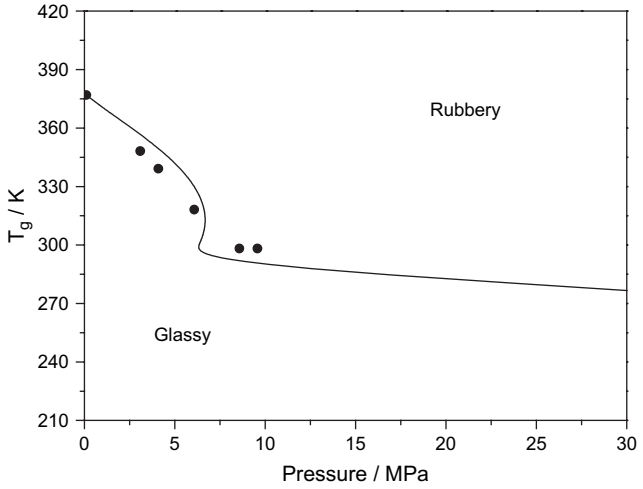

Fig. 17. Glass transition temperature for the PS–CO_2 system: (●) experimental data [31]; (—) NRHB.

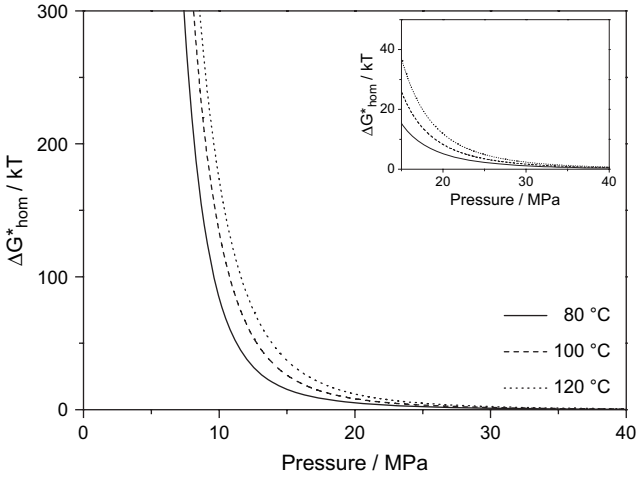

Fig. 18. Energy barrier for homogeneous nucleation in the PS–CO_2 system.

[21]. The parameters κ and β, that are needed in Eqs. (28) and (29), are characteristic for each fluid and were set equal to 0.121 and 2.00, respectively, values that were adopted from Ref. [21]. For the mixture calculations one binary interaction parameter, k_{12}, equal to 0.074 was used. This parameter was calculated by fitting the predictions of the theory to the experimental data for the sorption of CO_2 into polystyrene. Finally, the flex energy, u, in Eqs. (26) and (27) was calculated equal to 4102.9 J mol^{-1} by fitting the predictions of the theory to the experimental glass transition temperature of pure PS [21].

In the remaining correlations, one basic approximation was made. The pressure difference between the two sides of the bubble interface that is used in Eqs. (3) and (4) was set equal to the difference of the initial (the saturation pressure at the start of depressurization) and the final (the ambient) pressure [2,3]. This pressure difference reflects the supersaturation of the polymer matrix and the above approximation is valid only in the limit of very fast depressurization. Very high pressure drop rate was applied for the study of the effect of saturation pressure and foaming temperature. On the other hand, in order to study the effect of depressurization rate, porous structures were produced using both high and very low depressurization rates. As a consequence, the application of nucleation theory in order to predict the effect of depressurization rate is challenging indeed.

The energy barrier for homogeneous nucleation and the critical nuclei radius are presented in Figs. 18 and 19, respectively. The energy barrier for nucleation decreases exponentially with increase in pressure. This means that at higher saturation pressures nuclei are more easily generated inside the polymer matrix and consequently the final porous structure has more cells. This could explain the increase of the cell population density with increase of saturation pressure that was observed experimentally (see Fig. 5). The energy barrier for nucleation is very high at lower pressures and this could explain the difficulties of foaming polymers at such conditions [3]. On the contrary, the energy barrier reaches a plateau of very low values at higher pressures (greater than 30 MPa for the studied system) that could explain the leveling of cell density and pore size at these pressures (see Fig. 5).

On the other hand, at constant pressure the nucleation energy barrier increases with increase in temperature. The main reason for this is the implied increase of interfacial tension. It is reasonable to expect that as the temperature increases, the surface tension of the polymer matrix decreases. Nevertheless, as predicted from Eq. (30), this happens only at low pressures, where the sorption of CO_2 is not very high. At higher pressures the decrease of the CO_2 solubility that is caused by the temperature increase is more pronounced and results in an increase in the interfacial tension. Fig. 20 presents

Table 1
Scaling constants for pure fluids [21]

Fluid	ε^* (J mol^{-1})	v^* (cm^3 mol^{-1})	v^*_{sp} (cm^3 g^{-1})	s
CO_2	3040	5.970	0.707	0.909
PS	5828	8.418	0.916	0.667

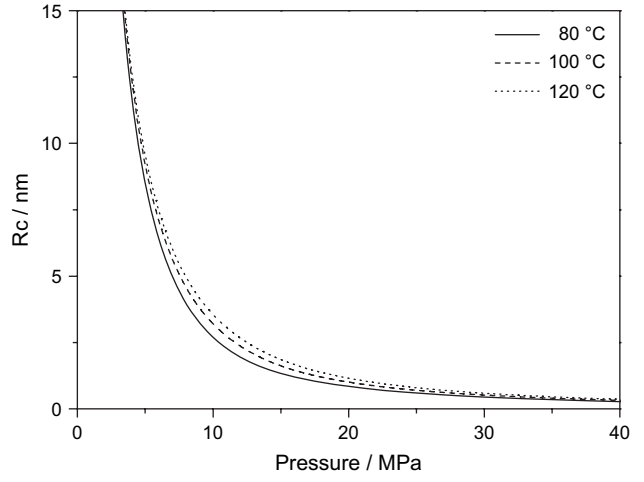

Fig. 19. Critical nucleus radius for homogeneous nucleation in the PS–CO_2 system.

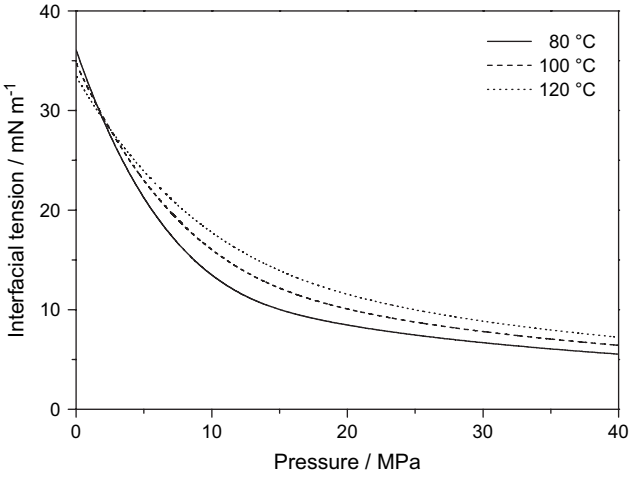

Fig. 20. Predicted interfacial tension of the system CO_2–PS.

the interfacial tension of the system CO_2–PS as predicted by Eq. (30).

As the energy barrier increases at higher temperatures, the generation of nuclei becomes more difficult and, consequently, fewer cells are observed in the final porous structure. This could explain the decrease of the cell population density with increase of the foaming temperature that was experimentally observed (see Figs. 9 and 10).

In previous studies [3,6], homogeneous nucleation theory proved is able to predict a pressure and temperature trend in nucleation similar to the trend of the experimentally observed cell population density. Usually, an adjustable parameter was incorporated in order to account for the growth or the coalescence of pores and subsequently the correlated nuclei density could be directly compared to the experimentally observed cell population density [3]. Nevertheless, often the process was only qualitatively described and not accurate correlations were obtained [3].

In this study, the nucleation theory was combined with NRHB model, in order to correlate the experimentally observed cell population density as a function of pressure and temperature. As previously described, the term ZR_{imp} of Eq.

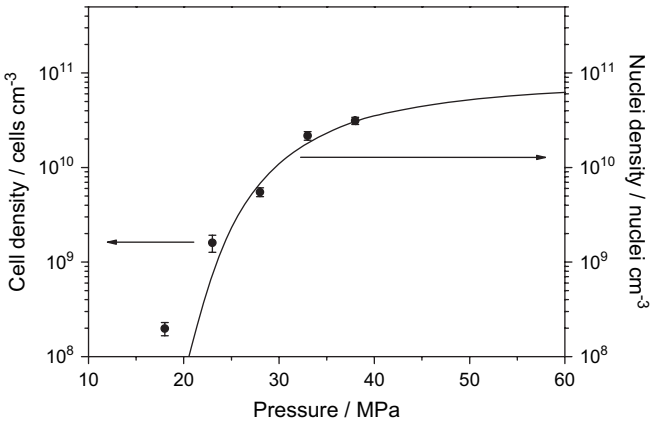

Fig. 21. Experimental cell population density (●), and calculated nuclei density (—), as function of pressure for PS–CO_2 system at 80 °C.

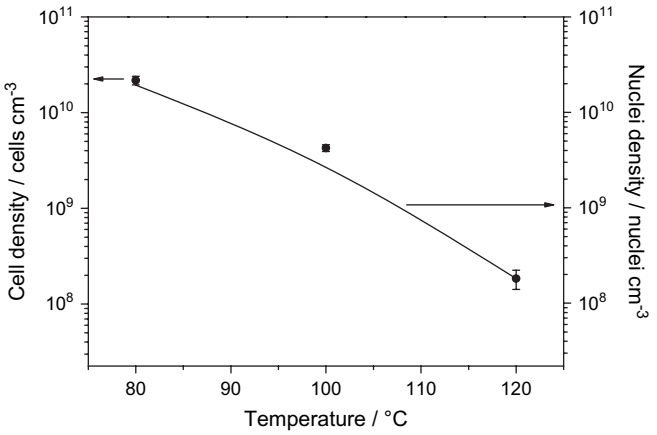

Fig. 22. Experimental cell population density (●), and calculated nuclei density (—), as function of temperature for PS–CO_2 system at 330 bar.

(6) served as temperature dependent adjustable parameter [3]. The results are summarized in Figs. 21 and 22. As observed, a good agreement between experimental and correlated values is obtained.

5. Conclusions

In this work microcellular PS foams and porous structures of the biodegradable $P_{D,L}LA$ were successfully prepared using supercritical CO_2 as a blowing agent. The results revealed that the size of the pores decreases and their population density increases with pressure increase, or decrease of temperature, and/or increase of the depressurization rate.

The results were correlated by combining nucleation theory with NRHB model. A satisfactory agreement between correlations and experimental data was obtained indicating that the nucleation theory not only describes qualitatively the foaming process but also yields quantitative correlations when variables such as sorption, degree of plasticization, and surface tension of the system polymer–supercritical fluid are accurately described.

Acknowledgement

Financial support by the Greek GSRT/PENED 2001 is gratefully acknowledged.

References

[1] Tomasko LD, Li H, Liu D, Han X, Wingert JM, Lee JL, et al. Ind Eng Chem Res 2003;42:6431–56.
[2] Kumar V, Suh NP. Polym Eng Sci 1990;30:1323–9.
[3] Goel SK, Beckman EJ. Polym Eng Sci 1994;34:1137–47.
[4] Arora KA, Lesser AJ, McCarthy JT. Macromolecules 1998;31:4614–20.
[5] Baldwin DF, Park CB, Suh NP. Polym Eng Sci 1996;36:1437–45.
[6] Siripurapu S, DeSimone JM, Khan SA, Spontak RJ. Adv Mater 2004;16:989–94.
[7] Mooney DJ, Baldwin DF, Suh NP, Vacati JP, Langer R. Biomaterials 1996;17:1417–22.
[8] Ma PX. Mater Today 2004;7:30–40.

[9] Siripurapu S, Coughlan JA, Spontak RJ, Khan SA. Macromolecules 2004;37:9872–9.
[10] Stafford CM, Russel TP, McCarthy JT. Macromolecules 1999;32: 7610–6.
[11] Liang M-T, Wang C-M. Ind Eng Chem Res 2000;39:4622–6.
[12] Xanthos M, Yilmazer U, Dey SK, Quintans J. Polym Eng Sci 2000;40:554–66.
[13] Singh L, Kumar V, Ratner BD. Biomaterials 2004;25:2611–7.
[14] Cotugno S, di Maio E, Mensitieri G, Iannace S, Roberts GW, Carbonell RG, et al. Ind Eng Chem Res 2005;44:1795–803.
[15] Tsivintzelis I, Pavlidou E, Panayiotou C. J Supercrit Fluids 2007;42: 265–72.
[16] Jenkins MJ, Harrison KL, Silva M, Whitaker MJ, Shakesheff KM, Howdle SM. Eur Polym J 2006;42:3145–51.
[17] Wang X, Li W, Kumar V. Biomaterials 2006;27:1924–9.
[18] Ema Y, Ikeya M, Okamoto M. Polymer 2006;47:5350–9.
[19] Colton JS, Suh NP. Polym Eng Sci 1987;27:500–3.
[20] Kumar V, Suh NP. Polym Eng Sci 1990;30:1323–9.
[21] Panayiotou C, Stefanis E, Tsivintzelis I, Pantoula M, Economou I. Ind Eng Chem Res 2004;43:6592–606.
[22] Panayiotou C, Tsivintzelis I, Economou IG. Ind Eng Chem Res 2007;46:2628–36.
[23] Quirk RA, France RM, Shakesheff KM, Howdle SM. Curr Opin Solid State Mater Sci 2004;8:313–21.
[24] Gabbard RG. The development of a homogeneous nucleation rate model for the thermoplastic foams based on a molecular partition function and fickian diffusion. Ph.D. thesis, New Jersey Institute of Technology, Department of Chemical Engineering, New Jersey; 2002.
[25] Gunton JD. J Stat Phys 1999;95:903–21.
[26] Pantoula M, Panayiotou C. J Supercrit Fluids 2005;37:254–62.
[27] Gibbs JH, DiMarzio EA. J Chem Phys 1958;28:373–83.
[28] Goel SK, Beckman EJ. Polym Eng Sci 1994;34:1148–56.
[29] Guo Q, Wang J, Park BC. Ind Eng Chem Res 2006;45:6153–61.
[30] Sato Y, Yurugi M, Fujiwara K, Takishima S, Masuoka H. Fluid Phase Equilib 1996;125:129–38.
[31] Dritsas SG, Tsivintzelis I, Panayiotou C. In: Lalia-Kantouri M, editor. Proceedings of the seventh Mediterranean conference on calorimetry and thermal analysis (MEDICTA 2005). Thessaloniki; 2005. p. 123–28.
[32] Li H, Lee LJ, Tomasko DL. Ind Eng Chem Res 2004;43:509–14.
[33] Park H, Park CB, Tzoganakis C, Tan KH, Chen P. Ind Eng Chem Res 2006;45:1650–8.
[34] Reid R, Prausnitz JM, Poling BE. The properties of gases and liquids. 4th ed. Singapore: McGraw-Hill international editions; 1988.